

Banner appropriate to article type will appear here in typeset article

Quantitative thermodynamic analyses of nucleation, evolution and stabilization of surface nanobubbles

Lili Lan¹, Yongcai Pan², Liang Zhao^{3,†}, and Binghai Wen^{1,2,‡}

¹College of Physical Science and Technology, Guangxi Normal University, Guilin 541004, China

²Key Lab of Education Blockchain and Intelligent Technology, Ministry of Education, Guangxi Normal University, Guilin 541004, China

³College of Physical Science and Technology, Yangzhou University, Jiangsu, 225009, China

(Received xx; revised xx; accepted xx)

Surface nanobubbles are complex micro- and nanoscale fluid systems. While thermodynamics is believed to dominate nanobubble dynamics, the precise mechanism by which nanobubble evolution is driven by thermodynamics remains unclear. It is essential to understand how nanobubble nucleation and growth, nanoscale contact line movement, and gas diffusion across the liquid-bubble interface are simultaneously driven by the change in free energy, leading to the ultimate thermodynamic equilibrium of surface nanobubble systems. In this paper, we first propose a quantitative theoretical model to elucidate the thermodynamic dominance behind the dynamics and stability of the fluid system with surface nanobubbles. The present model demonstrates that thermodynamic non-equilibrium drives the gas diffusion and the contact line motion of surface nanobubbles. Overcoming the nucleation energy barrier is crucial for bubble nucleation and growth. Surface nanobubbles evolve towards the reduction of the system's free energy and stabilize at the state with minimum free energy. The thermodynamic equilibrium is accompanied by the mechanical equilibrium at the contact line and the gas diffusion equilibrium at the liquid-bubble interface, and the theoretical results are in excellent agreement with the nanobubble morphology observed in experiments. The study highlights the significant influence of gas properties and ambient conditions in promoting bubble nucleation and stability.

Key words: bubble dynamics, nano-fluid dynamics

1. Introduction

Surface nanobubbles (SNBs) are spherical cap-shaped nanoscopic gaseous domains that form at the solid-liquid interface, representing a complex micro- and nanoscale fluid system (Lohse & Zhang 2015*b*; Tan *et al.* 2021; Zhou *et al.* 2021). Since being experimentally confirmed, the remarkable stability of SNBs has drawn significant interest from interfacial

† Email address for correspondence: zhaoliang@yzu.edu.cn

‡ Email address for correspondence: oceanwen@gxnu.edu.cn

Abstract must not spill onto p.2

scientists and engineers. This exceptional stability contradicts the widely accepted Epstein-Plesset theory (Epstein & Plesset 1950), which predicts that sub-micron nanobubbles would dissolve within microseconds. Understanding why SNBs can survive for days and weeks, and how they grow or shrink, is crucial for studying and utilizing nanobubbles in both experiments and industrial applications (Zhang & Lohse 2014; Lohse 2018). Essentially, the stability of SNBs is a thermodynamic issue. Although some pioneering studies have explained the nanobubble stability from a dynamic viewpoint (Lohse & Zhang 2015a; Tan *et al.* 2018; Wen *et al.* 2022), a comprehensive understanding of the nucleation, evolution and stabilization of surface nanobubbles requires a thermodynamic perspective.

A comprehensive review (Tan *et al.* 2021) highlights the challenge of resolving the stability of nanobubbles within a thermodynamic framework. These problems have been attempted to be solved by examining the conditions for the spontaneous growth of bubbles based on the second law of thermodynamics. Liu & Zhang (2013, 2018) proved the thermodynamic stability of pinned nanobubbles using lattice density functional theory in the grand canonical ensemble. Attard's theoretical analysis (Attard 2015, 2016) showed that only the pinned surface bubbles can minimize the system's free energy at the critical radius. Gadea *et al.* (2023) ingeniously used a finite-sized hydrophobic disk as the substrate. Their results demonstrate that when the contact line slides to the disk's edge and becomes pinned, the pinned bubble minimizes the system's free energy in an open environment. Regarding the stability of unpinned nanobubbles, Ward & Levart (1984) in their earlier study showed that the stable state of bubble nuclei is a result of mutual competition with the dissolved gas in the liquid phase within a closed volume. Then, Zargazadeh & Elliott (2016, 2019) addressed the free energy of SNBs as a function of size, identifying thermodynamically stable and metastable states for bubbles ranging from hundreds of nanometers to a few micrometers. These treatments examine the nucleation of multiple identical nanobubbles in a container with a finite amount of gas molecules, and also considers a realistic case where both the solute gas and the solvent are present in the liquid and bubble phases. In the above studies, gas diffusion and nanobubble dynamics processes have yet to be considered.

Scientists explain the dynamic stability of surface nanobubbles (SNBs) by primarily focusing on the behavior of the three-phase contact line and the gas flow at the liquid-bubble interface. The main characteristics of the movement of bubble contact lines include: pinning (Liu & Zhang 2013), self-pinning (Wang *et al.* 2009b; Ren *et al.* 2020; Guo *et al.* 2019; Chen *et al.* 2020) and unpinning (Petsev *et al.* 2020). Recently, Petsev *et al.* (2020) considered that the adsorption of gas molecules to the substrate lowered the solid-gas interface energy and explained the flat morphology of nanobubbles from a thermodynamic perspective. The bubble-liquid interface was found to be gas permeable by German *et al.* (2014), the gas diffusion through the interface drives the growth or shrinkage of SNBs. Brenner & Lohse (2008) suggested a dynamic equilibrium mechanism that the gas attracted by the hydrophobic walls influx at the contact line can compensate for the gas outflow. The gas diffusion from a surface nanobubble is analogous to the evaporation of a pinned drop, which was exactly solved by Popov (2005). Incorporating Henry's law into Popov's solution, Lohse & Zhang (2015a) derived the mass change of a pinned nanobubble in a supersaturated liquid. Then, Tan *et al.* (2018) introduced the potential into the pinning model and further explained the experimental observations that surface nanobubbles could survive in undersaturated environments (An *et al.* 2016; Qian *et al.* 2018). Moreover, experimental phenomena manifest that contact line pinning is not strictly necessary for the mechanical equilibrium of SNBs (Nag *et al.* 2021; Bull *et al.* 2018). Wen *et al.* (2022) proposed dynamic models for SNBs on homogeneous and heterogeneous surfaces, which can describe the state transition from the stable nanobubbles to unstable microbubbles (Pan *et al.* 2022; Lan *et al.* 2025).

In this study, we integrate a non-equilibrium drive for gas diffusion with an analysis of the

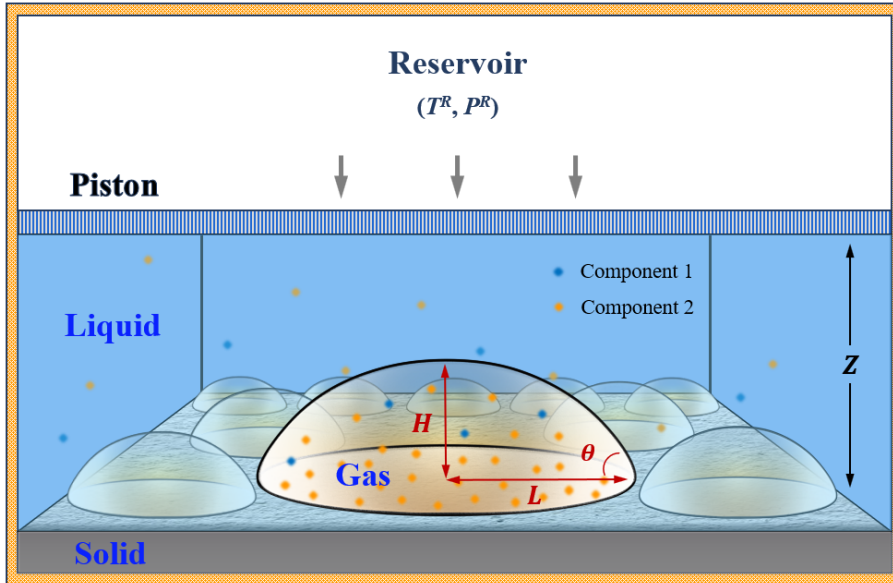


Figure 1: Schematic of closed fluid system with nanobubbles formed on a smooth solid surface submerged in a liquid-gas solution. The nanobubble morphology is characterized by three geometric parameters: footprint radius L , height H and bubble-side contact angle θ . The reservoir has the constant temperature T^R and the constant pressure P^R . A movable piston seals the liquid and keeps its pressure at the same level as the reservoir. The area of the solid substrate is A^S , and Z represents the initial height of the liquid phase. The liquid contains two types of particles: component 1 and component 2.

system's free energy changes, present quantitative thermodynamic calculations to investigate the critical nucleation, evolution direction, and stable state of SNBs in a closed environment. The gas adsorption effect at the solid-gas interface is introduced. Furthermore, the SNB morphology is examined for several common types of gases, taking into account the different actual gas properties.

2. Model

An isothermal-isobaric ensemble (NPT) is provided for the quantitative thermodynamic analysis of the SNB system. As shown in [Figure 1](#), the SNB system consists of the solid, liquid, and gas (bubble) phases, as well as the interfaces between them (Ward & Levart 1984; Zargarzadeh & Elliott 2016). The SNB system is in contact with a reservoir by means of a movable piston, which seals it off from the reservoir, and maintains its temperature and pressure at the same level as to the reservoir, thus creating a closed, constant temperature and pressure environment.

The closed SNB system, together with the external reservoir, can be considered as an isolated system in which the total internal energy, total volume and total particle number are conserved. According to the second law of thermodynamics, the total entropy of the system increases for any change towards equilibrium. Thus, the system's free energy B , also known as the thermodynamic potential, can be expressed by (Ward & Levart 1984; Zargarzadeh & Elliott 2016)

$$B = G^L + F^G + F^{LG} + F^{SL} + F^{SG} + P^L V^G, \quad (2.1)$$

where G and F denote the Gibbs and Helmholtz functions, P and V denote the pressure and

the sum of SNB volume. The superscripts R, L, G, LG, SL, and SG, represent the reservoir, liquid, gas (bubble), liquid-gas, solid-liquid, and solid-gas phases, respectively. Equation (2.1) indicate that the free energy for the SNB system is not solely one of the conventional thermodynamic potentials, the detailed process is presented in the supplementary materials.

This study considers two components in the closed liquid environment: water (H₂O) as component 1, and a specific gas that can dissolve in the water as component 2, denoted by subscripts. Therefore, Equation (2.1) can be calculated as

$$B = \left(\mu_1^L n_1^L + \mu_2^L n_2^L \right) + \left(\mu_1^G n_1^G + \mu_2^G n_2^G - P^G V^G \right) + \left(\mu_1^{LG} n_1^{LG} + \mu_2^{LG} n_2^{LG} + \gamma^{LG} A^{LG} \right) + \left(\mu_1^{SL} n_1^{SL} + \mu_2^{SL} n_2^{SL} + \gamma^{SL} A^{SL} \right) + \left(\mu_1^{SG} n_1^{SG} + \mu_2^{SG} n_2^{SG} + \gamma^{SG} A^{SG} \right) + P^L V^G, \quad (2.2)$$

where μ is chemical potential, n is the molecular number, γ is the interface tension, and A is the interface area. The SNB system in a completely liquid state, i.e. all the gas is dissolved in the liquid, is chosen as the reference, with relevant parameters denoted by subscript "0". So that the free energy of the system with respect to the reference can be defined by

$$\Delta B = \gamma^{LG} \left(A^{LG} - A^{SG} \cos \theta \right) - \left(P^G - P^L \right) V^G + N_1 \left(\mu_1^L - \mu_{10} \right) + N_2 \left(\mu_2^L - \mu_{20} \right) + \left(n_2^G + n_2^{LG} + n_2^{SG} \right) \left(\mu_2^G - \mu_2^L \right), \quad (2.3)$$

where N_1 and N_2 represent the total number of water and specific gas molecules in the SNB system. Compared to Ward's thermodynamic model, our study comprehensively explores the process of the system state transition from thermodynamic non-equilibrium to equilibrium. As depicted in Equation (2.3), the system's dynamic evolution is propelled by the chemical potential difference $\mu_2^G - \mu_2^L$ between the component 2 gas in bubbles and liquid, resulting in gas diffusion at the bubble-liquid interface. This process drives the growth or shrinkage of surface nanobubbles. It is clear that when the system reaches equilibrium, $\mu_2^G = \mu_2^L$ and the surface nanobubbles become stable. In this spontaneous process, the system's free energy decreases, allowing the evolution to continue until ΔB reaches a minimum that satisfies the given constraints. The criterion for the system being in a thermodynamic equilibrium state is that ΔB is a minimum (Ward & Levart 1984; Zargarzadeh & Elliott 2016).

Introducing the calculation of the chemical potential in each phase, Equation (2.3) can be further expressed as follows:

$$\Delta B = \gamma^{LG} \left(A^{LG} - A^{SG} \cos \theta \right) - \left(P^G - P^L \right) V^G + N_1 k_B T \left(\frac{N_2}{N_1} - \frac{n_2^L}{n_1^L} \right) + N_2 k_B T \ln \left(\frac{n_2^L}{n_{2s}^L} \frac{N_{2s0}}{N_{20}} \right) + \left(n_2^G + n_2^{LG} + n_2^{SG} \right) k_B T \ln \left(\frac{P^G}{P^L} \frac{n_{2s}^L}{n_2^L} \right), \quad (2.4)$$

where k_B is the Boltzmann constant, the subscript "s" indicates a gas-saturated state in liquid. Equation (2.4) shows that the change in the system's free energy is influenced by the real-time morphology of SNBs and the molecular distributions in each phase. The nanobubble shape is determined by the mechanical equilibrium at three-phase contact line and the gas molecular number in the bubble, which is adjusted by the gas diffusion across the liquid-bubble interface. The thermodynamic non-equilibrium drives the gas diffusion and the contact line motion of surface nanobubbles, and it is crucial for the quantitative thermodynamic analyses to calculate the gas diffusion rate and the nanobubble morphology in real time.

The distribution of the component 2 gas within the bubbles follows ideal gas properties (Ward & Levart 1984; Zargarzadeh & Elliott 2016; Attard 2016; Petsev *et al.* 2020). We

consider the Langmuir adsorption effect (Szyszkowski 1908; Swenson & Stadie 2019) of the component 2 gas molecular on the solid surface, thus the adsorbed molecular number is calculated by

$$n_2^{\text{SG}} = \frac{A^{\text{SG}}}{b} \left(\frac{KP_2^{\text{G}}}{1 + KP_2^{\text{G}}} \right), \quad (2.5)$$

where b is the cross-sectional area of a single adsorbing molecule, and K is the equilibrium adsorption constant in units of inverse pressure, and P_2^{G} is the partial pressures of component 2 gas in bubble. The gas adsorption generally lowers the solid-gas interface tension, and then the Young-Laplace equation needs to be modified by the Szyszkowski equation (Szyszkowski 1908) which is thermodynamically equivalent to the Langmuir adsorption isotherm (Swenson & Stadie 2019). The gas-side contact angle with the mechanical equilibrium, as well as the height and footprint radius, can be given by the implicit equation,

$$\cos \theta = \cos \Theta + \frac{k_{\text{B}}T}{b\gamma^{\text{LG}}} \ln \left(\frac{1 + KP_2^{\text{G}}}{1 + KP^{\text{L}}} \right), \quad (2.6)$$

where Θ is the macroscopic gas-side contact angle that symbolizes the degree of wettability of substrate surface ($\Theta < 90^\circ$ is hydrophobic, otherwise is hydrophilic).

Gas diffusion in the liquid can be considered as a quasistatic limit, and the gas concentration field c around the SNBs follows the quasistatic diffusion equation $\partial_t c = D\nabla^2 c \approx 0$, where D is the diffusion constant (Attard 2013). Lohse & Zhang (2015a) combined Popov's equation (Popov 2005) and Henry's law to calculate the diffusion rate of a pinned surface nanobubble. Molecular dynamics simulations have shown that the timescale for molecules' thermal motion to equilibrate a contact angle is within nanoseconds (Guo *et al.* 2019; Wang *et al.* 2009a; Maheshwari *et al.* 2016), which is more than three orders of magnitude faster than the diffusion timescale. From the perspective of diffusion, surface nanobubbles always retain the mechanical equilibrium during dynamic growth or shrinkage. Therefore, Wen *et al.* (2022) constrained the dynamic bubble morphology changed by the gas diffusion during the bubble evolution on a homogeneous substrate. By introducing Equation (2.6), the diffusion rate of component 2 gas molecules within the SNBs is derived as

$$\frac{dn_2^{\text{G}}}{dt} = -\frac{\pi D c_s}{m} L \left(\frac{2\gamma^{\text{LG}}}{HP^{\text{L}}} \left(1 - \cos \Theta - \frac{k_{\text{B}}T}{b\gamma^{\text{LG}}} \ln \left(\frac{1 + KP_2^{\text{G}}}{1 + KP^{\text{L}}} \right) \right) - \zeta(H, \theta) \right) f(\theta), \quad (2.7)$$

where $\zeta(H, \theta)$ represents the dynamic gas oversaturation in the liquid during bubble evolution. c_s is the solubility of gas, m is the gas molar mass, and $f(\theta)$ is a geometric term (Popov 2005). When the gas diffusion reaches equilibrium, i.e. $dn_2^{\text{G}}/dt = 0$, the SNBs reach a stable state.

Equation (2.6) imposes mechanical equilibrium constraints on the three-phase contact line, controlling the shape changes of the SNBs; while Equation (2.7) describes the diffusion direction and rate of gas molecules at the gas-liquid interface, driving the growth and contraction of the SNBs. Therefore, by substituting the changes in the particle number in each phase and the accompanying changes in bubble morphology into Equation (2.4), we can quantitatively analyze the dynamic system's free energy changes during the nucleation, growth, contraction, and stabilization of SNBs.

3. Results and discussion

We consider a nanobubble system, in which $q = 1 \times 10^{12}$ nanobubbles are evenly distributed on a surface with $A^{\text{S}} = 1 \text{ m}^2$. The initial height of the liquid phase is $Z = 1 \text{ }\mu\text{m}$. The

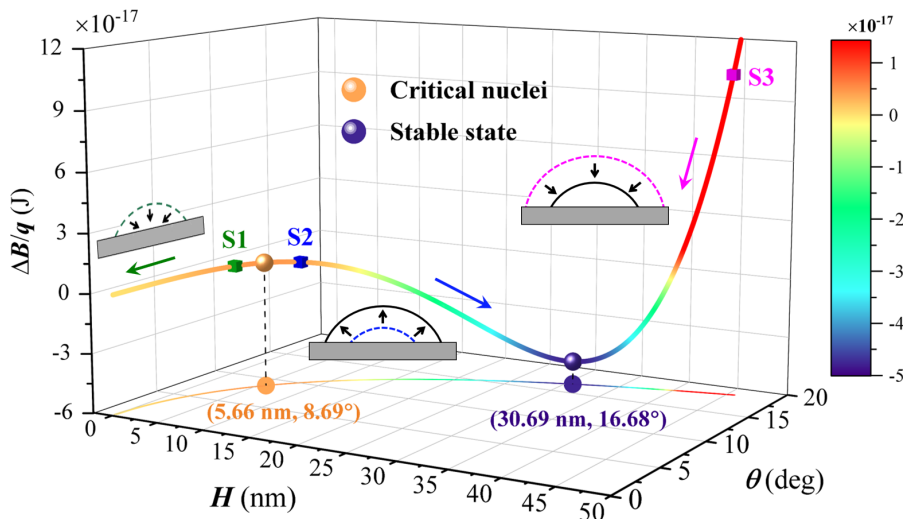


Figure 2: 3D image of system's free energy versus surface nanobubble size (height H and contact angle θ). The symbols of maximum (orange sphere) and minimum (dark purple sphere) free energy corresponds to critical nucleation and equilibrium state of a surface nanobubble, respectively. Three sample points, S1 (green square), S2 (blue square) and S3 (magenta square), are taken as the initial bubble states.

reservoir keeps at a constant room temperature $T^R = 25^\circ\text{C}$ and the standard atmospheric pressure $P^R = 1 \text{ atm}$.

3.1. Dynamics and stability of surface nanobubbles

In this section, Nitrogen (N_2) is considered as the component 2 gas for quantitative analysis, with $\gamma^{\text{LG}} = 0.072 \text{ N} \cdot \text{m}^{-1}$, $D = 2 \times 10^{-9} \text{ m}^2/\text{s}$, and $b = 7.548 \times 10^{-2} \text{ nm}^2$ (Lohse & Zhang 2015a; Petsev *et al.* 2020). By solving Equation (2.4), the relationship between the system free energy and nanobubble sizes can be obtained. The 3D curve of system's free energy change presented in Figure 2 illustrates the average impact of each SNB size (height H and contact angle θ) on the system free energy $\Delta B/q$, with gas adsorption strength $K = 5 \times 10^{-7}$, gas oversaturation $\zeta = 3$ and surface macroscopic gas-side contact angle $\Theta = 27^\circ$. In the $H - \theta$ axis plane, as the bubble grows, the height H and contact angle θ show a positive correlation. As shown in Figure 2, as the bubble height H and size increases, gas molecules in the liquid continuously flow into the bubble phase, resulting in a trend of initially increasing and then decreasing and then increasing system free energy, the change in the system's free energy exhibits a maximum state (represented by the orange sphere) and a minimum state (represented by the dark purple sphere). In thermodynamic description, the maximum of the system's free energy is regarded as the critical nucleation energy barrier for surface bubbles, corresponding to the bubble's critical nucleation size projected onto the $H - \theta$ axis plane. Only when the bubble grows to that size and overcomes the corresponding critical energy barrier, can the bubble continue to grow, otherwise it will dissolve. The system with the minimum of free energy is considered to be the most stable state. For the SNB system, the point of minimum free energy in Figure 2 should correspond to the most stable size of the surface nanobubble. Then, we take three sample points, S1 (green square), S2 (blue square), S3 (magenta square), as the initial states of SNBs to analyze their evolution.

In Figure 2, the orange sphere marking the free energy maximum point projected onto the $H - \theta$ axis plane corresponds to the SNB size of $H = 5.66 \text{ nm}$ and $\theta = 8.69^\circ$. The initial bubble size in S1 is $H = 5 \text{ nm}$ and $\theta = 7.42^\circ$, it is smaller than the critical nucleation

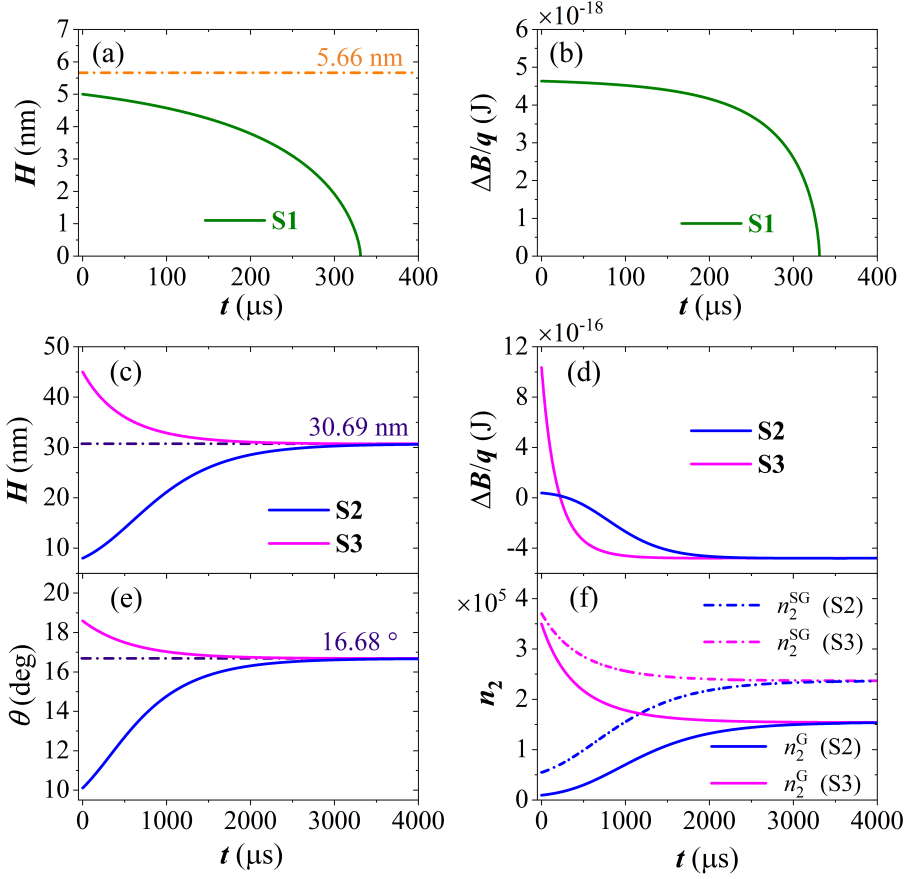


Figure 3: Evolution of (a) height H of S1 nanobubble, and (b) the corresponding system's free energy $\Delta B/q$ over time. Evolution of (c) height H of S2 and S3 nanobubbles, (d) the corresponding system's free energy $\Delta B/q$, (e) contact angle θ , and (f) molecular number n_2 of component 2 gas in bubble phase n_2^G and at adsorbed phase n_2^{SG} over time.

size. The dynamic processes of SNBs can be accurately calculated by using gas diffusion Equation (2.7). Figure 3(a) illustrates that S1 nanobubbles which have not yet reached the critical nucleation height are incapable of nucleating and growing, instead shrinking over time until they fully dissolve. In this process, the system's free energy continuously decreases, eventually returning to the reference state with no bubbles forming, as shown in Figure 3(b).

In Figure 2, the dark purple sphere marks the minimum value of the system free energy $\Delta B/q = -4.80 \times 10^{-16}$ J, and the corresponding SNB size projected onto the $H - \theta$ axis plane is $H = 30.69$ nm, $\theta = 16.68^\circ$. The initial sizes of nanobubbles in S2 and S3 are taken on either side of the bubble size corresponding to the minimum value of free energy cure in Figure 2. The blue curves in Figure 3(c) ~ (f) depict a growing S2 nanobubble starting at 8 nm height, while the magenta curves show the shrinking S3 nanobubble starting at 45 nm height. The changes in the blue curves indicate that as gas molecules continuously flow into the bubble from the liquid, the height H and contact angle θ of the S2 SNBs increase with time. Conversely, the magenta curves show that as gas molecules flow out of the bubble, the height and contact angle of the S3 SNBs decrease with time. Figure 3(d) illustrates that nanobubbles evolve in a direction that reduces the system's free energy, and they eventually

reach a stable state where the evolution curve becomes horizontal, indicating equilibrium in gas diffusion. This stable state aligns with the state of system's free energy minimum value depicted in [Figure 2](#). This evolution phenomenon indicates that the stable state of SNBs is characterized by minimizing the system's free energy. Any deviation in bubble shape will eventually lead it back to the stable state as gas diffuses. In addition, [Figure 3\(f\)](#) shows that when gas diffusion reaches equilibrium, the number of gas molecules adsorbed at the solid-bubble interface (dashed line) exceeds that in the bubble phase (solid line), indicating an ultra-dense aggregation of gas molecules at the bubble-substrate interface. This phenomenon is commonly observed in many molecular dynamic simulations (Chen *et al.* 2018; Yen *et al.* 2021).

Our thermodynamic model is capable of calculating the changes in system's free energy at any moment and state during the SNB evolution, caused by the gas diffusion. The analyses indicate that the evolution of SNBs consistently progresses towards reducing the system's free energy. When the bubble evolution reaches a stable equilibrium and the gas molecule flux at the bubble-liquid interface becomes zero, the system's free energy is minimized. The result highlights that a stable SNB must satisfy the unification of mechanical equilibrium at three-phase contact line, gas diffusion equilibrium at bubble-liquid interface, and system's thermodynamic equilibrium.

3.2. Nucleation and stability of nanobubbles in response to environmental conditions

In experiments, methods such as electrolysis and alcohol-water exchange (Seddon & Lohse 2011; Zhang & Lohse 2023) are commonly used to adjust the gas concentration in the solution in order to supersaturate or locally supersaturate it. This leads the aggregation of target gas molecules on the solid surface, forming surface nanobubbles. Recent nucleation rate experiments have revealed that the critical nucleus size for heterogeneous nanobubble formation ranges from 5 to 35 nm, much smaller than the bubbles observed by microscopy and studied theoretically (Attard 2016; Yatsyshin & Kalliadasis 2021; Yang *et al.* 2013). [Figure 4](#) investigates how different levels of gas oversaturation (with $\Theta = 25^\circ$ and $K = 2 \times 10^{-7}$) affect the nucleation and stability of surface nanobubbles. As shown in [Figure 4](#), the system's free energy curve gradually shifts downward with increasing gas oversaturation ζ in the liquid. [Figure 4\(b1\)](#) and [Figure 4\(b2\)](#) further demonstrate the alterations in the critical nucleation energy barrier and critical nucleation size of SNBs for different ζ values. The dot-line trends indicate that increasing gas concentration in the solution can lower the critical nucleation energy barrier and decrease the bubble nucleation size, thereby promoting the formation of surface nanobubbles. In the case of sufficient gas oversaturation, the nucleation barrier can disappear, leading to spontaneous nucleation of bubbles. For the stable state of SNBs, [Figure 4\(d1\)](#) illustrates that increased gas concentration leads to a lower minimum value of the system's free energy, resulting in larger stable nanobubbles. Additionally, [Figure 4\(d2\)](#) shows that as the bubble size increases, the gas partial pressure P_2^G in the bubble phase gradually decreases, resulting in a decrease in the adsorbed gas molecular density ρ_2^{SG} at the solid-bubble interface and a weakening of the gas adsorption strength.

In [Figure 4\(c1\)](#) and [Figure 4\(c2\)](#), the initial height of nanobubbles on the solid surface is 14 nm, which is between the critical nucleation heights of 14.59 nm at $\zeta = 4$ and 12.59 nm at $\zeta = 4.2$. This indicates that in the liquid conditions with a gas oversaturation of $\zeta = 4$ or lower, the initial nanobubble size does not reach the nucleation size. [Figure 4\(c2\)](#) illustrates that bubbles gradually shrink and dissolve in the liquid over time, with gas diffusing outward faster as the gas oversaturation decreases. Conversely, under the liquid condition with gas oversaturation of $\zeta = 4.2$ or higher, as shown in [Figure 4\(c1\)](#), nanobubbles continue to grow and eventually stabilize at an equilibrium state. The growth rate of nanobubbles

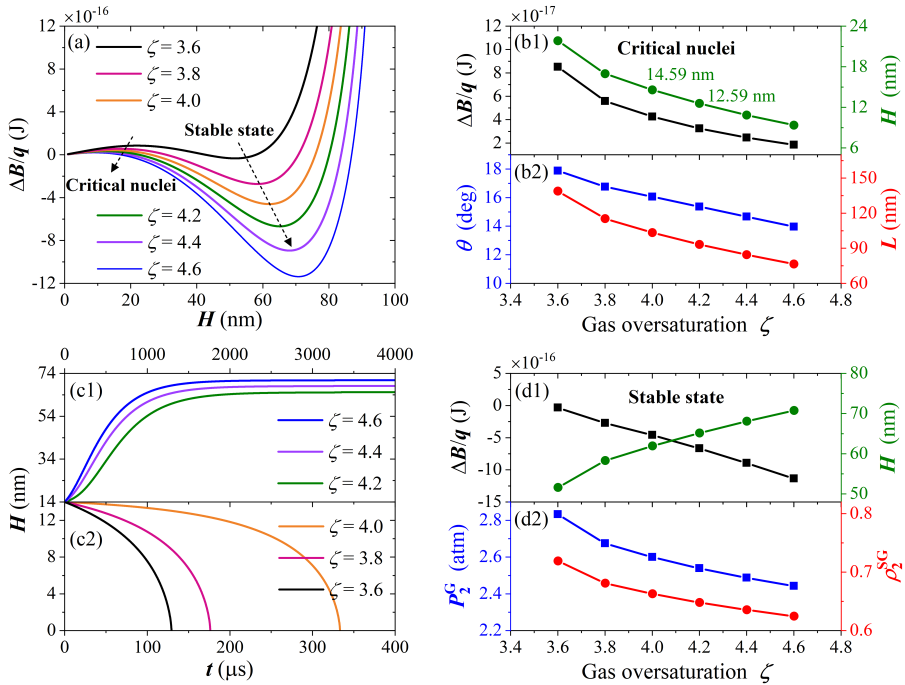


Figure 4: (a) System's free energy versus bubble height H for different gas oversaturation ζ . (b1) Energy barrier and bubble height H , (b2) contact angle θ and footprint radius L of surface nanobubble in the critical nucleation state versus gas oversaturation. (c1) (c2) Evolution of surface nanobubbles starting at 14 nm height over time for different gas oversaturation. (d1) System's free energy and bubble height H , (d2) gas partial pressure P_2^G in bubble phase and adsorbed gas molecular density ρ_2^{SG} at solid-bubble interface of surface nanobubble in the stable state versus gas oversaturation.

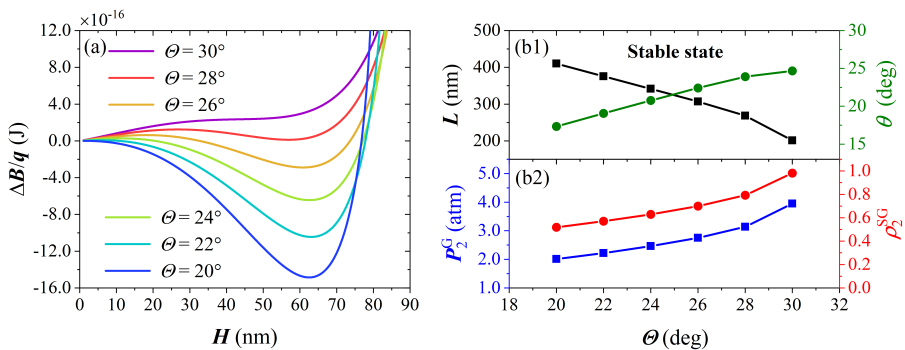


Figure 5: (a) System's free energy versus bubble height H for different macroscopic contact angles θ of substrate surface. (b1) Footprint radius L and contact angle θ , (b2) gas partial pressure P_2^G in bubble phase and adsorbed gas molecular density ρ_2^{SG} at solid-bubble interface of surface nanobubble in the stable state versus θ .

increases with higher gas oversaturation levels. Figure 4 demonstrates that increasing gas oversaturation not only lowers the critical nucleation barrier of bubbles, but also reduces the system's free energy in the stable state, allowing SNBs to survive more stably without being easily destroyed.

Figure 5 quantitatively analysis the impact of substrate hydrophobicity on the stable states

Parameter/Gas	H ₂	O ₂	N ₂	CO ₂	Air
γ^{LG} (N · m ⁻¹)	0.025	0.063	0.072	0.051	0.072
c_s (kg/nm ³)	0.00016	0.048	0.017	0.819	0.022
b (nm ²)	1.08×10^{-3}	8.04×10^{-2}	7.55×10^{-2}	8.52×10^{-2}	7.55×10^{-2}

Table 1: The gas-liquid interface tension γ^{LG} , the gas solubility c_s in liquid, and the cross-sectional area b of a single adsorbing molecule for H₂, O₂, N₂, CO₂, Air.

of surface nanobubbles, with $\zeta = 4$ and $K = 2 \times 10^{-7}$. **Figure 5(a)** demonstrates that reducing the macroscopic gas-side contact angle θ of the solid surface causes a downward shift in the free energy curve, suggesting the existence of stable bubbles with lower system free energy. In **Figure 5(b1)**, as θ decreases, the solid surface energy also decreases, indicating increased hydrophobicity. This leads to stable nanobubbles with a smaller contact angle and larger footprint radius, resulting in a flatter shape. **Figure 5(b2)** shows that the flatter shape of bubbles reduces the Laplace pressure, while the decreasing gas partial pressure P_2^{G} within the bubbles reduces the adsorbed gas molecular density ρ_2^{SG} at the solid-bubble interfaces. The analysis suggests that hydrophobic solid surfaces promote the formation and stability of SNBs, resulting in bubbles with a flatter shape.

In experiments and simulations (Lohse & Zhang 2015b), the formation and stability of surface nanobubbles are closely influenced by environmental factors, such as increased gas concentration, enhanced hydrophobicity of the substrate surface. These factors can compensate for each other to promote the nucleation and stability of nanobubbles on the solid surface. Therefore, the proposed thermodynamic model can effectively analyze the influence of the surrounding environment in which SNBs exist on their dynamics and stable forms, thereby shedding light on their prolonged existence.

3.3. Morphology and stability of nanobubbles with different gases

SNB morphology is also closely related to the gas type and properties. In experimental preparations, common gas types include: H₂ (Hydrogen) (Mita *et al.* 2022; German *et al.* 2018), O₂ (Oxygen) (Mita *et al.* 2022; Yang *et al.* 2009), N₂ (Nitrogen) (Yang *et al.* 2009; Zhang *et al.* 2006), CO₂ (Carbon dioxide) (Zhang *et al.* 2008; German *et al.* 2014), Air (Borkent *et al.* 2009; Zhang *et al.* 2010). **Figure 6** compares the characteristics of SNBs on a hydrophobic HOPG (highly oriented pyrolytic graphite, with $\theta = 85^\circ$) substrate formed by five different gases in terms of bubble morphology and stability. Due to the differences in gas properties, here, H₂ with $K = 1 \times 10^{-7}$, and the other with $K = 1 \times 10^{-5}$. **Table 1** lists the parameter values of the five gases, including gas-liquid interfacial tension γ^{LG} , the gas solubility c_s in liquid, and the cross-sectional area b of a single gas molecule.

In **Figure 6(a)**, the system free energy curves for five gas nanobubbles show that when the system is in equilibrium at the minimum free energy state, the stable H₂ nanobubble is the most stable, with in same initial gas oversaturation $\zeta = 6$. The CO₂ nanobubbles are the most unstable, in other words, it is difficult for them to be stable at the nanoscale, which is consistent with the observation that CO₂ SNBs are typically at the micrometer scale in experimental measurements (German *et al.* 2014). The stable size of N₂, Air, and O₂ nanobubbles increases in sequence, and their stability also increases in sequence. **Figure 6(c1)** and **6(c2)** show the evolution of height and contact angle of H₂, O₂, N₂ nanobubbles from nucleation, growth, to stabilization processes, it can be observed that O₂ nanobubbles take longer to reach larger stable sizes. In addition, under the same footprint radius L , stable H₂ nanobubbles present better stability and a flatter morphology, as shown in **Figure 6(b)** and

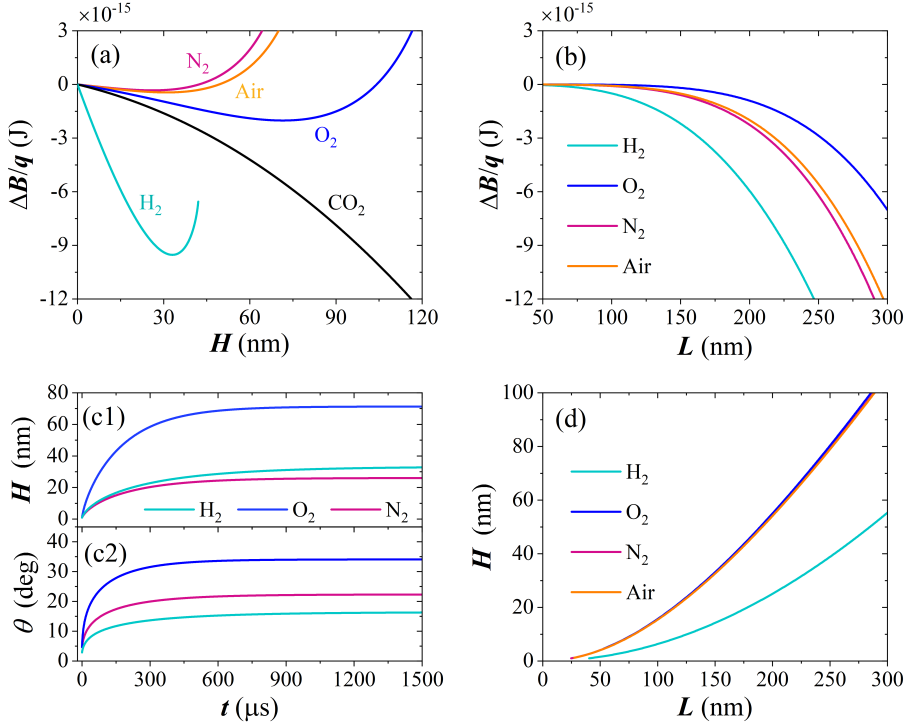


Figure 6: (a) System's free energy versus bubble height H for H_2 , O_2 , N_2 , CO_2 , Air nanobubbles on hydrophobic HOPG surfaces. (b) System's free energy versus footprint radii L of H_2 , O_2 , N_2 , Air nanobubble in stable equilibrium state. (c) Evolution of height H and contact angle θ of H_2 , O_2 , N_2 nanobubble over time. (d) Height H versus footprint radii L of H_2 , O_2 , N_2 , Air nanobubble in stable equilibrium state.

Figure 6(d). The experiments of Mita *et al.* (2022) clearly illustrated the characteristic of H_2 SNBs: those with a flatter shape are less mobile and tend to maintain a fixed position.

Figure 7(a) and **Figure 7(b)** show the system free energy curves of Air and H_2 (Hydrogen) nanobubbles on the HOPG surface, the spheres mark the stable state of nanobubbles at the minimum system free energy. The changes in the free energy curves indicate that as the gas oversaturation ζ in the liquid increases, the stable SNBs have larger sizes and stronger stability. It can be observed that the stable state curve of SNBs is connected by red circles, which are projected onto the height H and contact angle θ plane by the free energy minimum points. In Experiment, Zhang *et al.* (2010) generated Air and H_2 nanobubbles on the hydrophobic HOPG surface using the alcohol-water exchange method and the electrolysis method, respectively. The size of SNBs distributed on the surface was measured using an atomic force microscope. The experimental data of Air and H_2 nanobubbles are represented by white and gray circles in the $H - \theta$ plane in **Figure 7(a)** and **Figure 7(b)**, respectively. Comparing the stable state curves and the experimental data for SNBs, the stable morphology of SNBs obtained by our thermodynamic model calculation closely aligns with the experimental phenomenon within an acceptable margin of error. This result strongly supports our theoretical research.

4. Conclusions

This study integrates a gas molecular diffusion model with thermodynamic analysis to explore the critical nucleation, evolution and stable state of surface nanobubbles in a closed

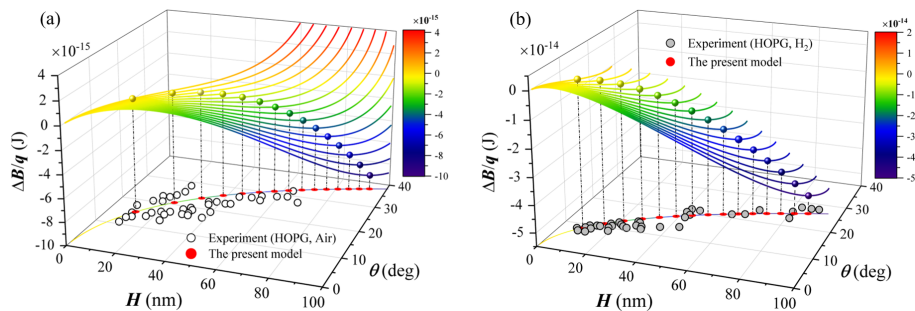


Figure 7: System's free energy versus bubble height H and contact angle θ as gas oversaturation increases for (a) Air and (b) H_2 nanobubbles on hydrophobic HOPG surface. The red circles projection of the spheres representing stable bubble states on the H - θ plane. The experimental data of (a) Air (white circles) and (b) H_2 (gray circles) nanobubbles on hydrophobic HOPG surfaces by Zhang *et al.* (2010)

environment. The gas adsorption effect at the bubble-substrate interface is also considered. The present model ensures that the stable surface nanobubbles unify the mechanical equilibrium at the contact line, the gas diffusion equilibrium at the bubble-liquid interface, and the thermodynamic equilibrium of the whole fluid system, leading to the formation of stable surface nanobubbles.

The analyses suggest that thermodynamic non-equilibrium drives the gas diffusion and the contact line motion of surface nanobubbles. Overcoming the nucleation energy barrier is crucial for bubble formation and growth. The evolved nanobubbles adhere to the contact line mechanical equilibrium and gas diffusion relations. They evolve in a manner that reduces the system's free energy, and are stabilized at the minimum free energy state. Surface nanobubbles are more likely to form and remain stable in environments with hydrophobic substrates and higher gas concentrations in the liquid, which can help explain their prolonged presence. In addition, the stable state curve of surface nanobubbles with minimum free energy predicted by the presented thermodynamic model is consistent with the experimental phenomenon. Under identical same environmental conditions, hydrogen nanobubbles exhibit a flatter shape and better stability.

The present model extends thermodynamic calculations to analyze the evolution of surface nanobubbles, providing valuable insights into the system's dynamic progression. This perspective provides stronger support for the stability explanation of surface nanobubbles and will be particularly valuable for the investigation of fluid motion and interfacial processes. In our upcoming research, based on the established thermodynamic model, we aim to further investigate the stability of surface nanobubbles by considering the gas supersaturation layer (Tan *et al.* 2018) and the resulting variations in the gas-water interfacial tension (Attard 2015, 2016).

Funding. This work was supported by the National Natural Science Foundation of China (Nos. 12272100, 11605151), and the Innovation Project of Guangxi Graduate Education (No. YCBZ2024087).

Declaration of interests. The authors report no conflict of interest.

Author ORCIDs. Liang Zhao, <https://orcid.org/0000-0003-2687-1026>; Binghai Wen, <https://orcid.org/0000-0002-0127-3268>.

REFERENCES

AN, HONGJIE, TAN, BENG HAU, ZENG, QINGYUN & OHL, CLAUDIUS-DIETER 2016 Stability of nanobubbles formed at the interface between cold water and hot highly oriented pyrolytic graphite. *Langmuir* **32** (43), 11212–11220.

- ATTARD, PHIL 2013 The stability of nanobubbles. *The European Physical Journal Special Topics* **223** (5), 893–914.
- ATTARD, PHIL 2015 Thermodynamic stability of nanobubbles.
- ATTARD, PHIL 2016 Pinning down the reasons for the size, shape, and stability of nanobubbles. *Langmuir* **32** (43), 11138–11146.
- BORKENT, BRAM M., DE BEER, SISSI, MUGELE, FRIEDER & LOHSE, DETLEF 2009 On the shape of surface nanobubbles. *Langmuir* **26** (1), 260–268.
- BRENNER, MICHAEL P. & LOHSE, DETLEF 2008 Dynamic equilibrium mechanism for surface nanobubble stabilization. *Physical Review Letters* **101** (21).
- BULL, DAVID S., NELSON, NATHANIEL, KONETSKI, DANIELLE, BOWMAN, CHRISTOPHER N., SCHWARTZ, DANIEL K. & GOODWIN, ANDREW P. 2018 Contact line pinning is not required for nanobubble stability on copolymer brushes. *The Journal of Physical Chemistry Letters* **9** (15), 4239–4244.
- CHEN, CHANGSHENG, ZHANG, XIANREN & CAO, DAPENG 2020 Role of substrate softness in stabilizing surface nanobubbles. *Green Energy & Environment* **5** (3), 374–380.
- CHEN, YI-XIAN, CHEN, YENG-LONG & YEN, TSU-HSU 2018 Investigating interfacial effects on surface nanobubbles without pinning using molecular dynamics simulation. *Langmuir* **34** (50), 15360–15369.
- EPSTEIN, P. S. & PLESSET, M. S. 1950 On the stability of gas bubbles in liquid-gas solutions. *The Journal of Chemical Physics* **18** (11), 1505–1509.
- GADEA, ESTEBAN D., MOLINERO, VALERIA & SCHERLIS, DAMIÁN A. 2023 Nanobubble stability and formation on solid–liquid interfaces in open environments. *Nano Letters* **23** (15), 7206–7212.
- GERMAN, SEAN R., EDWARDS, MARTIN A., REN, HANG & WHITE, HENRY S. 2018 Critical nuclei size, rate, and activation energy of h₂ gas nucleation. *Journal of the American Chemical Society* **140** (11), 4047–4053.
- GERMAN, SEAN R., WU, XI, AN, HONGJIE, CRAIG, VINCENT S. J., MEGA, TONY L. & ZHANG, XUEHUA 2014 Interfacial nanobubbles are leaky: Permeability of the gas/water interface. *ACS Nano* **8** (6), 6193–6201.
- GUO, ZHENJIANG, WANG, XIAN & ZHANG, XIANREN 2019 Stability of surface nanobubbles without contact line pinning. *Langmuir* .
- LAN, LILI, PAN, YONGCAI, ZHOU, LIMIN, KUANG, HUA, ZHANG, LIJUAN & WEN, BINGHAI 2025 Theoretical model of dynamics and stability of nanobubbles on heterogeneous surfaces. *Journal of Colloid and Interface Science* **678**, 322–333.
- LIU, YAWEI & ZHANG, XIANREN 2013 Nanobubble stability induced by contact line pinning. *The Journal of Chemical Physics* **138** (1).
- LIU, YAWEI & ZHANG, XIANREN 2018 A review of recent theoretical and computational studies on pinned surface nanobubbles. *Chinese Physics B* **27** (1), 014401.
- LOHSE, DETLEF 2018 Bubble puzzles: From fundamentals to applications. *Physical Review Fluids* **3** (11).
- LOHSE, DETLEF & ZHANG, XUEHUA 2015a Pinning and gas oversaturation imply stable single surface nanobubbles. *Physical Review E* **91** (3).
- LOHSE, DETLEF & ZHANG, XUEHUA 2015b Surface nanobubbles and nanodroplets. *Reviews of Modern Physics* **87** (3), 981–1035.
- MAHESHWARI, SHANTANU, VAN DER HOEF, MARTIN, ZHANG, XUEHUA & LOHSE, DETLEF 2016 Stability of surface nanobubbles: A molecular dynamics study. *Langmuir* **32** (43), 11116–11122.
- MITA, MASHU, MATSUSHIMA, HISAYOSHI, UEDA, MIKITO & ITO, HIROSHI 2022 In-situ high-speed atomic force microscopy observation of dynamic nanobubbles during water electrolysis. *Journal of Colloid and Interface Science* **614**, 389–395.
- NAG, SARTHAK, TOMO, YOKO, TESHIMA, HIDEAKI, TAKAHASHI, KOJI & KOHNO, MASAMICHI 2021 Dynamic interplay between interfacial nanobubbles: oversaturation promotes anisotropic depinning and bubble coalescence. *Physical Chemistry Chemical Physics* **23** (43), 24652–24660.
- PAN, YONGCAI, ZHOU, LIMIN & WEN, BINGHAI 2022 The stability and morphology of nanobubbles on homogeneous surfaces with different wettability. *Physics of Fluids* **34** (7).
- PETSEV, NIKOLAI D., LEAL, L. GARY & SHELL, M. SCOTT 2020 Universal gas adsorption mechanism for flat nanobubble morphologies. *Physical Review Letters* **125** (14).
- POPOV, YURI O. 2005 Evaporative deposition patterns: Spatial dimensions of the deposit. *Physical Review E* **71** (3).
- QIAN, JING, CRAIG, VINCENT S. J. & JEHANNIN, MARIE 2018 Long-term stability of surface nanobubbles in undersaturated aqueous solution. *Langmuir* **35** (3), 718–728.

- REN, SHUAI, PEDERSEN, CHRISTIAN, CARLSON, ANDREAS, SALEZ, THOMAS & WANG, YULIANG 2020 Capillary deformation of ultrathin glassy polymer films by air nanobubbles. *Physical Review Research* **2** (4).
- SEDDON, JAMES R T & LOHSE, DETLEF 2011 Nanobubbles and micropancakes: gaseous domains on immersed substrates. *Journal of Physics: Condensed Matter* **23** (13), 133001.
- SWENSON, HANS & STADIE, NICHOLAS P. 2019 Langmuir's theory of adsorption: A centennial review. *Langmuir* **35** (16), 5409–5426.
- SZYSZKOWSKI, BOHDAN VON 1908 Experimentelle studien über kapillare eigenschaften der wässrigen lösungen von fettsäuren. *Zeitschrift für Physikalische Chemie* **64U** (1), 385–414.
- TAN, BENG HAU, AN, HONGJIE & OHL, CLAUDI-DIETER 2018 Surface nanobubbles are stabilized by hydrophobic attraction. *Physical Review Letters* **120** (16).
- TAN, BENG HAU, AN, HONGJIE & OHL, CLAUDI-DIETER 2021 Stability of surface and bulk nanobubbles. *Current Opinion in Colloid & Interface Science* **53**, 101428.
- WANG, CHUNLEI, LU, HANGJUN, WANG, ZHIGANG, XIU, PENG, ZHOU, BO, ZUO, GUANGHONG, WAN, RONGZHENG, HU, JUN & FANG, HAIPING 2009a Stable liquid water droplet on a water monolayer formed at room temperature on ionic model substrates. *Physical Review Letters* **103** (13).
- WANG, YULIANG, BHUSHAN, BHARAT & ZHAO, XUEZENG 2009b Improved nanobubble immobility induced by surface structures on hydrophobic surfaces. *Langmuir* **25** (16), 9328–9336.
- WARD, C. A. & LEVART, EUGENE 1984 Conditions for stability of bubble nuclei in solid surfaces contacting a liquid-gas solution. *Journal of Applied Physics* **56** (2), 491–500.
- WEN, BINGHAI, PAN, YONGCAI, ZHANG, LIJUAN, WANG, SHUO, ZHOU, LIMIN, WANG, CHUNLEI & HU, JUN 2022 State transition of stable nanobubbles to unstable microbubbles on homogeneous surfaces. *Physical Review Fluids* **7** (10).
- YANG, CHIH-WEN, LU, YI-HSIEN & HWANG, ING-SHOUH 2013 Imaging surface nanobubbles at graphite–water interfaces with different atomic force microscopy modes. *Journal of Physics: Condensed Matter* **25** (18), 184010.
- YANG, SHANGJIONG, TSAI, PEICHUN, KOOIJ, E. STEFAN, PROSPERETTI, ANDREA, ZANDVLIET, HAROLD J. W. & LOHSE, DETLEF 2009 Electrolytically generated nanobubbles on highly orientated pyrolytic graphite surfaces. *Langmuir* **25** (3), 1466–1474.
- YATSYSHIN, PETER & KALLIADASIS, SERAFIM 2021 Surface nanodrops and nanobubbles: a classical density functional theory study. *Journal of Fluid Mechanics* **913**.
- YEN, TSU-HSU, LIN, CHIA-HE & CHEN, YENG-LONG 2021 Effects of gas adsorption and surface conditions on interfacial nanobubbles. *Langmuir* **37** (8), 2759–2770.
- ZARGARZADEH, LEILA & ELLIOTT, JANET A. W. 2016 Thermodynamics of surface nanobubbles. *Langmuir* **32** (43), 11309–11320.
- ZARGARZADEH, LEILA & ELLIOTT, JANET A. W. 2019 Bubble formation in a finite cone: More pieces to the puzzle. *Langmuir* **35** (40), 13216–13232.
- ZHANG, LIJUAN, ZHANG, XUEHUA, ZHANG, YI, HU, JUN & FANG, HAIPING 2010 The length scales for stable gas nanobubbles at liquid/solid surfaces. *Soft Matter* **6** (18), 4515.
- ZHANG, LIJUAN, ZHANG, YI, ZHANG, XUEHUA, LI, ZHAOXIA, SHEN, GUANGXIA, YE, MING, FAN, CHUNHAI, FANG, HAIPING & HU, JUN 2006 Electrochemically controlled formation and growth of hydrogen nanobubbles. *Langmuir* **22** (19), 8109–8113.
- ZHANG, XUEHUA & LOHSE, DETLEF 2014 Perspectives on surface nanobubbles. *Biomicrofluidics* **8** (4).
- ZHANG, XUE HUA, QUINN, ANTHONY & DUCKER, WILLIAM A. 2008 Nanobubbles at the interface between water and a hydrophobic solid. *Langmuir* **24** (9), 4756–4764.
- ZHANG, YIXIN & LOHSE, DETLEF 2023 Minimum current for detachment of electrolytic bubbles. *Journal of Fluid Mechanics* **975**.
- ZHOU, LIMIN, WANG, SHUO, ZHANG, LIJUAN & HU, JUN 2021 Generation and stability of bulk nanobubbles: A review and perspective. *Current Opinion in Colloid & Interface Science* **53**, 101439.